CHEMISTRY
A EUROPEAN JOURNAL

DOI: 10.1002/chem.200701465

Linear Polynuclear Helicates as a Link between Discrete Supramolecular Complexes and Programmed Infinite Polymetallic Chains

Natalia Dalla-Favera,[a] Josef Hamacek,[a] Michal Borkovec,[a] Damien Jeannerat,[b] Frédéric Gumy,[c] Jean-Claude G. Bünzli,[c] Gianfranco Ercolani,[d] and Claude Piguet*[a]

Abstract: The contribution of the solvation energies to the assembly of polynuclear helicates reduces the free energy of intermetallic repulsion, ΔE^{MM}, in condensed phase to such an extent that stable D_3-symmetrical tetranuclear lanthanide-containing triple-stranded helicates $[Ln_4(\mathbf{L4})_3]^{12+}$ are quantitatively produced at millimolar concentrations, despite the twelve positive charge borne by these complexes. A detailed modelling of the formation constants using statistical factors, adapted to self-assembly processes involving intra- and intermolecular connections, provides a set of five microscopic parameters, which can be successfully used for rationalizing the stepwise generation of linear bi-, tri- and tetranuclear analogues. Photophysical studies of $[Eu_4(\mathbf{L4})_3]^{12+}$ confirm the existence of two different binding sites producing differentiated metal-centred emission at low temperature, which transforms into single site luminescence at room temperature because of intramolecular energy funelling processes.

Keywords: helical structures · multicomponent assembly · polynuclear · statistical factors · thermodynamics

Introduction

A challenge in supramolecular chemistry is the development of a rational bottom-up process, which would produce nanoscopic, or even macroscopic objects from the assembly of molecular edifices obeying some simple rules based on molecular recognition processes.[1] The latter approach is particularly attractive when specific properties and functions can be amplified by the supramolecular interactions operating between the building blocks in the self-assembled edifices. For instance, sophisticated multifunctional photophysical devices based on inter-connected $[Ru(2,2'\text{-bipyridine})_3]^{2+}$ derivatives benefit from supramolecular energy funnelling pathways,[2] while artificial machines and motors,[3] nano-imprinted devices,[4] and programmed luminescent liquid crystals[5] could not be designed without a significant increase in molecular complexity.

However, the rationalization of the underlying multicomponent assemblies is still limited to some semiempirical transcriptions of macroscopic intuition into the microscopic domain, while statistical mechanics, the natural tool for connecting micro- and macroscopic worlds, is usually not considered (we use the word "microscopic" in the usual way, that is, as opposed to "macroscopic", while it really means "molecular or atomic scale"). Except for some remarkable attempts, which aim at correlating the intriguing stabilities of multicomponent assemblies with preorganization and cooperativity concepts,[4,6] we are aware of a single case, in which the transfer matrix formalism, inherited from statistical mechanics, has been used to predict the partition function of simple one-dimensional chains of charged metal ions bound to a single receptor.[7] Starting from the modelling of

[a] N. Dalla-Favera, Dr. J. Hamacek, Prof. Dr. M. Borkovec, Prof. Dr. C. Piguet
Department of Inorganic, Analytical and Applied Chemistry
University of Geneva, 30 quai E. Ansermet
1211 Geneva 4 (Switzerland)
Fax: (+41) 22-379-6830
E-mail: Claude.Piguet@chiam.unige.ch

[b] Dr. D. Jeannerat
Department of Organic Chemistry, University of Geneva
30 quai E. Ansermet, 1211 Geneva 4 (Switzerland)

[c] F. Gumy, Prof. Dr. J.-C. G. Bünzli
Laboratory of Lanthanide Supramolecular Chemistry
École Polytechnique Fédérale de Lausanne
BCH 1402, 1015 Lausanne (Switzerland)

[d] Prof. Dr. G. Ercolani
Dipartimento di Scienze e Tecnologie Chimiche
Università di Roma Tor Vergata
Via della Ricerca Scientifica, 00133 Roma (Italy)

Supporting information for this article is available on the WWW under http://www.chemeurj.org/ or from the author: Equations (S1–S13), appendix, Tables S1–S3 and Figures S1–S6 corresponding to thermodynamic modeling, and structural and spectroscopic analyses.

the thermodynamic data relevant to the formation of linear binuclear $[Ln_2(\mathbf{L1})_3]^{6+}$,[8] $[Ln_2(\mathbf{L2})_3]^{6+}$[9] and trinuclear $[Ln_3(\mathbf{L3})_3]^{9+}$ helicates (Ln is a trivalent lanthanide, Figure 1),[10] statistical mechanics predicts that the binding isotherm of identical metal ions to a long linear receptor strongly depends on the nearest neighbour free-energy pair interaction ΔE_{1-2}^{LnLn}.[7] When $\Delta E_{1-2}^{LnLn}=0$, the binding sites are statistically occupied by the metals, thus leading to a

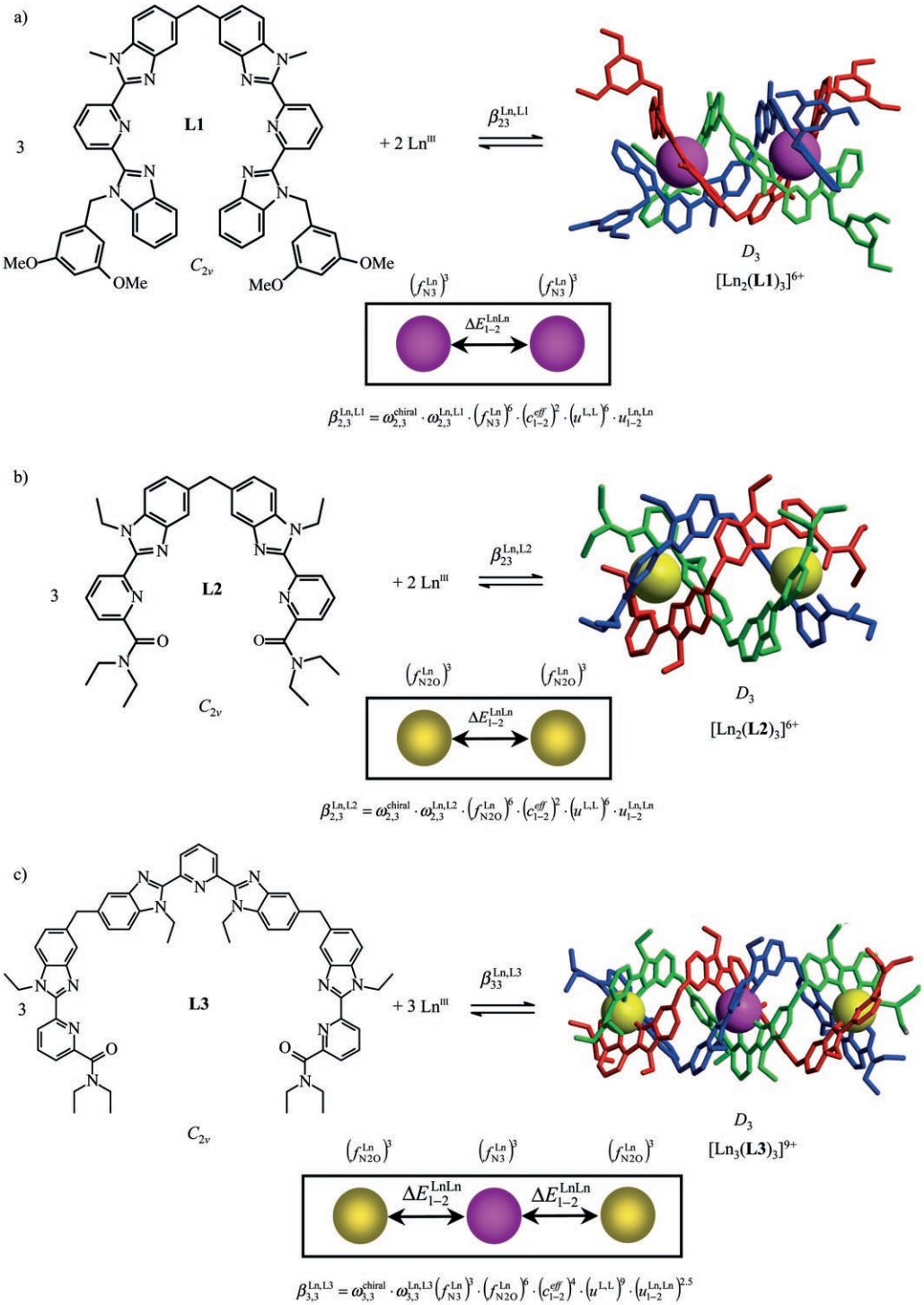

Figure 1. Self-assembly of the polynuclear triple-stranded helicates a) $[Ln_2(\mathbf{L1})_3]^{6+}$, b) $[Ln_2(\mathbf{L2})_3]^{6+}$, c) $[Ln_3(\mathbf{L3})_3]^{9+}$, and associated extended site-binding model $\omega_{mn}^{chiral}\cdot\omega_{mn}^{Ln,Lk}$ is the statistical factor of the assembly process, $(f_{N3}^{Ln})^3$ and $(f_{N2O}^{Ln})^3$ are the microscopic affinities of Ln^{III} for the tridentate N_9 (pink) and N_6O_3 (yellow) sites, respectively, c_{1-2}^{eff} is the so-called effective concentration adapted to the intramolecular ring closure of two neighboring sites, $\Delta E^{LL} = -RT\ln(u^{LL})$ and $\Delta E_{1-2}^{LnLn}=-RT\ln(u_{1-2}^{LnLn})$ represents the free energies for intramolecular interligand, respectively intermetallic interactions operating between two nearest neighbors).[7] The final helicates correspond to X-ray crystal structures.

random arrangement along the chain (Figure 2a, non-cooperative process). When $\Delta E_{1-2}^{LnLn} > 0$, the repulsive interaction between adjacent metals produces a plateau in the binding isotherm corresponding to the half occupancy of the sites, in which alternating empty and occupied sites are expected (Figure 2b, anti-cooperative process). Finally, $\Delta E_{1-2}^{LnLn} < 0$ relates to attractive neighbouring intermetallic interactions producing clusters of metals along the chains during the metal loading process (Figure 2c, cooperative process).

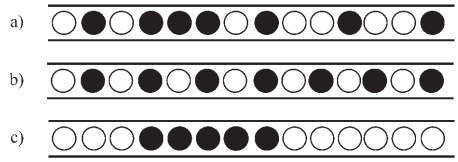

Figure 2. Pictorial representation of microstates of long linear receptors: a) random occupancy ($\Delta E_{1-2}^{LnLn}=0$), b) half-occupied receptor with alternating occupied and empty sites ($\Delta E_{1-2}^{LnLn} > 0$), and c) clusters of empty and occupied sites ($\Delta E_{1-2}^{LnLn} < 0$).

For the $[Ln_m(\mathbf{Lk})_3]^{3m+}$ ($k=1$–3) helicates, the experimental ΔE_{1-2}^{LnLn} values systematically correspond to weak repulsive intermetallic interactions and anti-cooperative behaviours.[11] However, some significant improvements of our understanding of the behaviour of discrete chains of metal ions in helicates have emerged during the past three years thanks to 1) the explicit consideration of intra- and intermolecular binding events in self-assembly processes,[12] which allows the estimation of physically meaningful intermetallic interactions ΔE_{1-2}^{LnLn} by using the extended site-binding model,[13] and 2) the partition of ΔE_{1-2}^{LnLn} between electrostatic and solvation effects, which opens perspectives for a quantitative interpretation of intercomponent interactions in condensed phases.[14] Consequently, the chemical tuning of ΔE_{1-2}^{LnLn} for programming selective organized sequences of lanthanides, or more generally metal ions, along a linear receptor remains a crucial unresolved challenge.

As a first step toward this goal, we report in this contribution on the thorough investigation of the tetranuclear D_3-symmetrical analogue $[Ln_4(\mathbf{L4})_3]^{12+}$ (Figure 3) which allows i) the assignment of adequate statistical factors for helicate self-assemblies involving intra- and intermolecular processes, ii) the collection of a sufficient amount of thermodynamic formation constants to reliably estimate the intramolecular intermetallic interactions (ΔE_{1-2}^{LnLn}), and iii) the design of a simple thermodynamic model for predicting the energetics of multicomponent metallosupramolecular assemblies. The syntheses of the ligand **L4** and of its complexes $[Ln_4(\mathbf{L4})_3](CF_3SO_3)_{12}$, and the crystal structure of $[Eu_4(\mathbf{L4})_3]^{12+}$ have been described in a preliminary communication.[15]

Results and Discussion

Quantitative predictions for the self-assembly of the tetranuclear helicate $[Eu_4(L4)_3]^{12+}$ in solution: The application of the extended site-binding model,[13] which holds for self-assembly processes involving intra- and intermolecular binding events, requires the consideration of one statistical factor $\omega_{m,n}^{chiral}\cdot\omega_{m,n}^{M,L}$ and four parameters ($f_i^{M,L}$, c_i^{eff}, $u_{i,j}^{MM}$, $u_{k,l}^{LL}$) for the description of any microscopic stability constant $\beta_{m,n}^{M,L}$ associated with the formation of the supramolecular complex $[M_mL_n]$ from its separated components [Eq. (1)].[13]

$$\begin{aligned}\beta_{m,n}^{M,L} &= e^{-(\Delta G_{m,n}^{M,L}/RT)} \\ &= \omega_{m,n}^{chiral}\cdot\omega_{m,n}^{M,L}\cdot\prod_{i=1}^{mn} f_i^{M,L}\cdot\prod_{i=1}^{mn-m-n+1} c_i^{eff}\cdot\prod_{i<j} u_{i,j}^{MM}\cdot\prod_{k<l} u_{k,l}^{LL}\end{aligned} \quad (1)$$

In this equation, $f_i^{M,L}$ represents the intermolecular microscopic affinity characterizing the connection of a metal M to the binding site i of a ligand **L**, $c_i^{eff}=e^{-(\Delta S_{i,inter}^{M,L}-\Delta S_{i,intra}^{M,L})/R}$ is the so-called effective concentration used for correcting the entropy change occurring in intramolecular connections, $u_{i,j}^{MM} = e^{-(\Delta E_{i,j}^{MM}/RT)}$ and $u_{k,l}^{LL}=e^{-(\Delta E_{k,l}^{LL}/RT)}$ are the *Boltzman*'s factors accounting for the intermetallic $\Delta E_{i,j}^{MM}$, respectively interligand $\Delta E_{k,l}^{LL}$, free energies of interaction operating in the final $[M_mL_n]$ complex.[13] Taking into account the two standard assumptions relevant to helicate self-assemblies with semi-rigid ligands, 1) no hairpin or constrained structures are formed and 2) the principle of maximum site occupancy is obeyed,[13] application of Equation (1) to the complexation

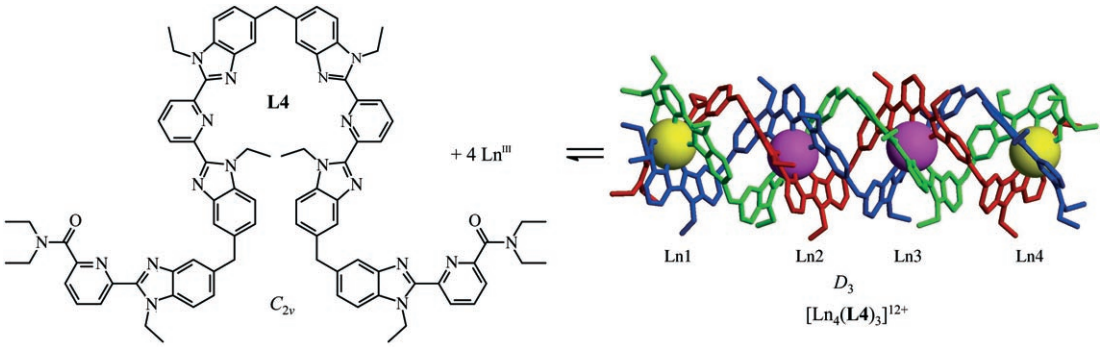

Figure 3. Self-assembly of the polynuclear triple-stranded helicates $[Ln_4(\mathbf{L4})_3]^{12+}$ (the LnN_9 sites are represented in pink and the LnN_6O_3 sites in yellow). The final helicates correspond to the X-ray crystal structure of $[Eu_4(\mathbf{L4})_3]^{12+}$.[15]

of the tetratridentate ligand **L4** with Eu^{III} to give $[Eu_4(\mathbf{L4})_3]^{12+}$ [Equilibrium (2)] provides a straightforward model for the associated formation constant $\beta_{4,3}^{Eu,\mathbf{L4}}$ [Eq. (3)].

$$3\,\mathbf{L4} + 4\,Eu^{3+} \rightleftharpoons [Eu_4(\mathbf{L4})_3]^{12+} \qquad \beta_{4,3}^{Eu,\mathbf{L4}} \tag{2}$$

$$\beta_{4,3}^{Eu,\mathbf{L4}} = \omega_{4,3}^{chiral}\cdot\omega_{4,3}^{Eu,\mathbf{L4}}\cdot(f_{N2O}^{Eu})^6\cdot(f_{N3}^{Eu})^6\cdot(c_{1-2}^{eff})^6\cdot(u_{1-2}^{EuEu})^3 \cdot(u_{1-3}^{EuEu})^2\cdot(u_{1-4}^{EuEu})\cdot(u^{LL})^{12} \tag{3}$$

$$\beta_{4,3}^{Eu,\mathbf{L4}} = \omega_{4,3}^{chiral}\cdot\omega_{4,3}^{Eu,\mathbf{L4}}\cdot(f_{N2O}^{Eu})^6\cdot(f_{N3}^{Eu})^6\cdot(c_{1-2}^{eff})^6 \cdot u_{(1-2}^{(EuEu)^{4.33}}\cdot(u^{LL})^{12} \tag{4}$$

The parameters f_{N2O}^{Eu} and f_{N3}^{Eu} represent the intermolecular microscopic affinities of Eu^{III} for the tridentate N_2O (terminal) and N_3 (central) binding sites of **L4**, respectively; c_{1-2}^{eff} is the entropic correction operating when the intramolecular cyclization involves two adjacent tridentate sites bound to Eu^{III} in the final metallomacrocycle. The dependence of c^{eff} on the distance is not trivial and an analytical formulation only exists for long flexible polymers (see Appendix, Supporting Information).[16] For highly flexible long polymers connecting two sites separated by a distance d in a receptor, $c^{eff} \propto d^{-1.5}$, while the use of a related polymer of optimized size leads to $c^{eff} \propto d^{-3}$.[16] The ligand strands in the triple stranded helicate $[Eu_4(\mathbf{L4})_3]^{12+}$ can be considered neither as long flexible nor as optimized polymeric chains, but are probably in between. The two limiting cases $c^{eff} \propto d^{-\alpha}$ ($\alpha =$ 1.5 or 3) are thus systematically considered in our model. We therefore calculate that $c_{1-3}^{eff} = c_{1-2}^{eff}/2^{\alpha}$ and $c_{1-4}^{eff} = c_{1-2}^{eff}/3^{\alpha}$ because the four binding sites are regularly spaced along the ligand strand. The parameter u_{1-2}^{EuEu} represents the intermetallic interaction occurring between two adjacent Eu^{III} separated by 9.054–9.405 Å as determined in the crystal structure of $[Eu_4(\mathbf{L4})_3]^{12+}$ (average 9.26(18) Å).[15] For the rigid assembly in question, a standard Coulombic approach predicts $\ln(u^{EuEu}) \propto$-const/d,[14] which leads to $u_{1-3}^{EuEu} = (u_{1-2}^{EuEu})^{0.5}$ and $u_{1-4}^{EuEu} = (u_{1-2}^{EuEu})^{0.33}$, because the metals are regularly spaced along the strand. Finally, the interligand interaction u^{LL} is restricted to operate between two sites bound to the same metal.[13] For instance, the complexation of each Eu^{III} ion in a nine-coordinate site in $[Eu_4(\mathbf{L4})_3]^{12+}$ provides three interligand interactions, thus leading to a total of $3\cdot4 = 12$ interligand interactions in the complex. Consequently, Equation (3) reduces to Equation (4), and the same approach can be applied for the modelling of the formation constants of the competitive complexes $[Eu_3(\mathbf{L4})_2]^{9+}$ [Eqs. (5–6)], $[Eu_3(\mathbf{L4})_3]^{9+}$ [Eqs. (7–8)] and $[Eu_4(\mathbf{L4})_2]^{12+}$ [Eqs. (9–10)], which are expected to exist for slightly different stoichiometries (the schematic structures of the $[Eu_m(\mathbf{L4})_n]^{3m+}$ complexes are shown in Figure 4; *t* stands for terminal, *c* for central and *s* for shifted).

$$2\,\mathbf{L4} + 3\,Eu^{3+} \rightleftharpoons [Eu_3(\mathbf{L4})_2]^{9+} \qquad \beta_{3,2}^{Eu,\mathbf{L4}} \tag{5}$$

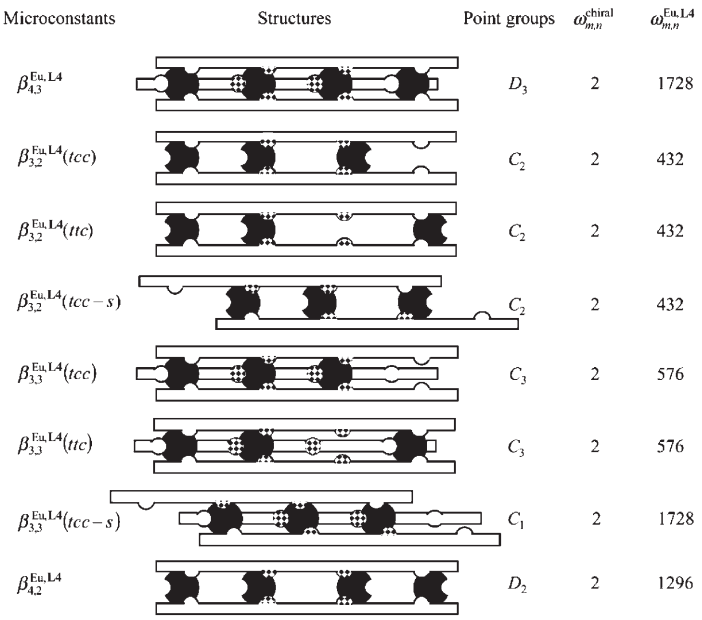

Figure 4. Schematic structures, symmetries and statistical factors for $[Eu_m(\mathbf{L4})_n]^{3m+}$ microspecies.

$$\begin{aligned}\beta_{3,2}^{Eu,\mathbf{L4}} &= \beta_{3,2}^{Eu,\mathbf{L4}}(tcc) + \beta_{3,2}^{Eu,\mathbf{L4}}(ttc) + \beta_{3,2}^{Eu,\mathbf{L4}}(tcc\text{-s})\\ &= \omega_{3,2}^{chiral}\cdot\omega_{3,2}^{Eu,\mathbf{L4}}(tcc)\cdot(f_{N2O}^{Eu})^2\cdot(f_{N3}^{Eu})^4\cdot(c_{1-2}^{eff})^2\cdot(u_{1-2}^{EuEu})^{2.5}\cdot(u^{LL})^3\\ &+\omega_{3,2}^{chiral}\cdot\omega_{3,2}^{Eu,\mathbf{L4}}(ttc)\cdot(f_{N2O}^{Eu})^4\cdot(f_{N3}^{Eu})^2\cdot(c_{1-2}^{eff})^2/2^{\alpha}\cdot(u_{1-2}^{EuEu})^{1.83}\cdot(u^{LL})^3\\ &+\omega_{3,2}^{chiral}\cdot\omega_{3,2}^{Eu,\mathbf{L4}}(tcc\text{-s})\cdot(f_{N2O}^{Eu})^2\cdot(f_{N3}^{Eu})^4\cdot(c_{1-2}^{eff})^2\cdot(u_{1-2}^{EuEu})^{2.5}\cdot(u^{LL})^3\end{aligned} \tag{6}$$

$$3\,\mathbf{L4} + 3\,Eu^{3+} \rightleftharpoons [Eu_3(\mathbf{L4})_3]^{9+} \qquad \beta_{3,3}^{Eu,\mathbf{L4}} \tag{7}$$

$$\begin{aligned}\beta_{3,3}^{Eu,\mathbf{L4}} &= \beta_{3,3}^{Eu,\mathbf{L4}}(tcc) + \beta_{3,3}^{Eu,\mathbf{L4}}(ttc) + \beta_{3,3}^{Eu,\mathbf{L4}}(tcc\text{-s})\\ &= \omega_{3,3}^{chiral}\cdot\omega_{3,3}^{Eu,\mathbf{L4}}(tcc)\cdot(f_{N2O}^{Eu})^3\cdot(f_{N3}^{Eu})^6\cdot(c_{1-2}^{eff})^4\cdot(u_{1-2}^{EuEu})^{2.5}\cdot(u^{LL})^9\\ &+\omega_{3,3}{}^{chiral}\cdot\omega_{3,3}^{Eu,\mathbf{L4}}(ttc)\cdot(f_{N2O}^{Eu})^6\cdot(f_{N3}^{Eu})^3\cdot(c_{1-2}^{eff})^4/2^{\alpha}\cdot(u_{1-2}^{EuEu})^{1.83}\cdot(u^{LL})^9\\ &+\omega_{3,3}^{chiral}\cdot\omega_{3,3}^{Eu,\mathbf{L4}}(tcc\text{-s})\cdot(f_{N2O}^{Eu})^3\cdot(f_{N3}^{Eu})^6\cdot(c_{1-2}^{eff})^4\cdot(u_{1-3}^{EuEu})^{2.5}\cdot(u^{LL})^9\end{aligned} \tag{8}$$

$$2\,\mathbf{L4} + 4\,Eu^{3+} \rightleftharpoons [Eu_4(\mathbf{L4})_2]^{12+} \qquad \beta_{4,2}^{Eu,\mathbf{L4}} \tag{9}$$

$$\beta_{4,2}^{Eu,\mathbf{L4}} = \omega_{4,2}^{chiral}\cdot\omega_{4,2}^{Eu,\mathbf{L4}}\cdot(f_{N2O}^{Eu})^4\cdot(f_{N3}^{Eu})^4\cdot(c_{1-2}^{eff})^3\cdot(u_{1-2}^{EuEu})^{4.33}\cdot(u^{LL})^4 \tag{10}$$

A set of five microscopic parameters $\log(f_{N2O}^{Eu}) = 5.9(2)$, $\log(f_{N3}^{Eu}) = 5.6(2)$, $\log(c_{1-2}^{eff}) = -0.9(9)$, $\log(u_{1-2}^{EuEu}) = -2.4(8)$ (i.e., $\Delta E_{1-2}^{EuEu} = 14(5)\ kJ\,mol^{-1}$) and $\log(u^{LL}) = -0.9(4)$ (i.e., $\Delta E^{LL} = 5(3)\ kJ\,mol^{-1}$) have been previously computed from the simultaneous non-linear least-squares fit of the experimental thermodynamic formation constants obtained for the complexes $[Eu_m(\mathbf{L1})_n]^{3m+}$, $[Eu_m(\mathbf{L2})_n]^{3m+}$ and $[Eu_m(\mathbf{L3})_n]^{3m+}$ (Table 1, column 2, the structures of the complexes are shown in Figure 1).[13b]

Table 1. Fitted microscopic thermodynamic parameters for $[Eu_m(\mathbf{L}k)_n]^{3m+}$ (simultaneous non-linear least-squares fits, acetonitrile, 298 K).

Microscopic parameters	$k=1$–3[a] Binomial statistics $\alpha=3$[b]	$k=1$–3 Symmetry numbers $\alpha=3$[b]	$k=1$–3 Symmetry numbers $\alpha=1.5$[b]	$k=1$–4 Symmetry numbers $\alpha=3$[b]	$k=1$–4 Symmetry numbers $\alpha=1.5$[b]
$\log(f_{N3}^{Eu,\mathbf{L}k})/\Delta g_{N3}^{Eu,\mathbf{L}k}$ [kJ mol^{-1}]	5.6(2)/−32(1)	5.1(2)/−29(1)	5.3(2)/−30(1)	5.3(2)/−30(1)	5.4(2)/−31(1)
$\log(f_{N2O}^{Eu,\mathbf{L}k})/\Delta g_{N2O}^{Eu,\mathbf{L}k}$ [kJ mol^{-1}]	5.9(2)/−34(1)	5.4(2)/−31(1)	5.6(2)/−32(1)	5.6(2)/−32(1)	5.7(2)/−33(1)
$\log(c^{eff})/\Delta g_{corr}^{Eu,\mathbf{L}k}$ [kJ mol^{-1}]	−0.9(9)/5(5)	−1.9(9)/11(5)	−1.5(9)/8.6(5)	−0.8(2)/5(1)	−1.0(9)/6(5)
$\log(u^{LL})/\Delta E^{LL}$ [kJ mol^{-1}]	−0.9(4)/5(2)	−0.6(3)/3(2)	−0.8(3)/5(2)	−1.4(3)/8(2)	−1.0(3)/6(2)
$\log(u_{1-2}^{EuEu})/\Delta E_{1-2}^{EuEu}$ [kJ mol^{-1}]	−2.4(8)/14(5)	−1.4(7)/8(4)	−1.8(7)/10(4)	−1.5(3)/9(2)	−1.8(7)/10(4)

[a] Taken from ref. [13b]. [b] Dependence of the effective concentration on the distance $c^{eff} \propto d^{-\alpha}$ ($\alpha=1.5$ or 3), see text.

However, the statistical factors $\omega_{m,n}^{chiral}\cdot\omega_{m,n}^{Eu,\mathbf{L}k}$ used for the latter calculation relied on combinatorial analyses based on binomial distributions, an approach limited to multicomponent assemblies involving only intermolecular binding processes.[13b] Recently,[17] it has been demonstrated that statistical factors adapted to assemblies mixing intra- and intermolecular connections can be obtained with the symmetry number method,[18] which fully agrees with the direct counting technique.[19] Let us apply these two methods for the calculation of the partial statistical factor $\omega_{4,3}^{Eu,\mathbf{L}k}$ characterizing the formation of the tetranuclear helicate $[Eu_4(\mathbf{L4})_3]^{12+}$ [Eq. (2)]. According to the symmetry number method, $\omega_{4,3}^{Eu,\mathbf{L4}}$ is given by the ratio between the products of the symmetry numbers of the reactants and that of the product species, taken to the power of their stoichiometric coefficients n_i [Eq. (11)].[18]

$$\omega_{4,3}^{Eu,\mathbf{L4}} = \prod_i (\sigma_i^{reactant})^{n_i} / \prod_j (\sigma_j^{product})^{n_j} = \frac{(\sigma_{\mathbf{L4}})^3\cdot(\sigma_{Eu})^4}{\sigma_{Eu_4(\mathbf{L4})_3}} \quad (11)$$

Each factor σ is itself the product of external σ^{ext} and internal σ^{int} symmetry numbers; σ^{ext} corresponds to the number of different, but indistinguishable atomic arrangements that can be obtained by rotating a molecule with symmetry operations of the first kind; σ^{int} refers to the same definition relevant to internal rotations about single bonds within a molecule. In order to calculate the symmetry numbers, the solvent molecules in the first coordination spheres of the metals must be explicitly considered, and the notation of Equation (2), which is common in supramolecular chemistry, must be replaced with Equation (12),[20] thus allowing the calculation of the statistical factor $\omega_{4,3}^{Eu,\mathbf{L4}}=1728$ [Eq. (13), Figure 4 entry 1].

$$3\,\mathbf{L4} + 4\,[Eu(CH_3CN)_9]^{3+} \rightleftharpoons [Eu_4(\mathbf{L4})_3]^{12+} + 36\,CH_3CN \qquad \beta_{4,3}^{Eu,\mathbf{L4}} \quad (12)$$

symmetry	C_{2v}	D_{3h}	D_3	$C_{\infty h}$
σ^{ext}	2	6	6	1
σ^{int}	1	3^9	1	3
σ^{chiral}	1	1	$^1/_2$	1

$$\omega_{4,3}^{Eu,\mathbf{L4}} = \frac{(\sigma_{\mathbf{L4}})^3\cdot(\sigma_{Eu})^4}{\sigma_{Eu_4(\mathbf{L4})_3}\cdot(\sigma_{CH_3CN})^{36}} = \frac{(2\cdot1)^3\cdot(6\cdot3^9)^4}{(6\cdot1)\cdot(1\cdot3)^{36}} = 1728 \quad (13)$$

The symmetry number of a chiral molecule present at equilibrium as a racemic mixture must be divided by two to account for the existence of two enantiomers with identical symmetry due to the entropy of mixing.[17] The latter effect can be introduced as a correction term $\omega_{m,n}^{chiral}$ given in Equation (14):

$$\omega_{4,3}^{chiral} = \frac{(\sigma_{\mathbf{L4}}^{chiral})^3\cdot(\sigma_{Eu}^{chiral})^4}{\sigma_{Eu_4(\mathbf{L4})_3}^{chiral}\cdot(\sigma_{CH_3CN}^{chiral})^{36}} = \frac{(1)^3\cdot(1)^4}{(1/2)\cdot(1)^{36}} = 2 \quad (14)$$

We thus conclude that the global statistical factor of Equilibrium (12) is given by $\omega_{4,3}^{chiral}\cdot\omega_{4,3}^{Eu,\mathbf{L4}} = 2\cdot1728 = 3456$ (Figure 4, entry 1). The same result can be obtained by the more intuitive, but more tedious, direct counting of microspecies.[19] In the latter method, the statistical factor of an equilibrium can be obtained by the ratio l/r, whereby l is the number of microspecies in the products that can be formed if all identical atoms in the reactants are labeled, and r represents the reverse situation, that is, the number of microspecies in the reactants that can be formed if all identical atoms in the products are labeled.[19] Let us apply this technique to the statistical factor related to the formation of $[Eu_4(\mathbf{L4})_3]^{12+}$ [Eq. (2)] obtained by the reaction of four metals considered as simple flat tripodal connectors (D_{3h} symmetry, three labels A1, A2, A3), and three ligands acting as linkers with four successive connection points (C_{2v} symmetry, labels B1-C-C-B2, Figure 5). Since all metals and ligands are combined to give the single species $[Eu_4(\mathbf{L4})_3]^{12+}$, the factor l is simply defined as the degeneracy of the final complex. The three labels A1, A2, A3 of each trigonal connector (i.e. metal), can be arranged clockwise (plus, P) or anticlockwise (minus, M), thus leading to 16 different arrangements in the final helicate (Figure 5, column 1): P_4 ($C_0^4=1$ possibility), P_3M ($C_1^4=4$ possibilities, P_2M_2 ($C_2^4=6$ possibilities), M_3P ($C_3^4=4$ possibilities) and M_4 ($C_4^4=1$ possibility). For each chiral organization of the metals, there are

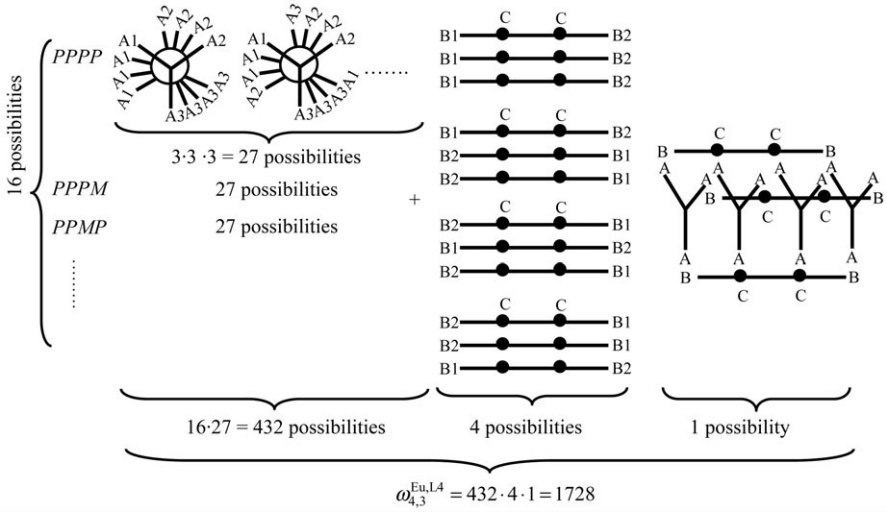

Figure 5. Schematic illustration of the calculation of the statistical factor $\omega_{4,3}^{Eu,\mathbf{L4}}$ by using the direct count method for the tetrametallic helicate $[Eu_4(\mathbf{L4})_3]^{12+}$.

$3^{(4-1)} = 27$ different relative orientations of the four aligned tripods with respect to rotation about the intermetallic axis (Figure 5, column 2). Finally, there are four possible arrangements of the three ligands corresponding to head-to-head-to-head (1 possibility, three identical labels located at the termini of the three ligand strands) and head-to-head-to-tail organizations (3 possibilities, different labels located at the termini of the three ligand strands, Figure 5, column 3). We thus calculate $l = 16 \cdot 27 \cdot 4 = 1728$ microspecies characterizing the complex $[Eu_4(\mathbf{L4})_3]^{12+}$, while there is only $r = 1$ way for dissociating the final helicate to give the separated reactants. The partial statistical factor is thus simply obtained $\omega_{4,3}^{Eu,\mathbf{L4}} = l/r = 1728$, in agreement with the method of the symmetry numbers. The arrangement of the three strands in the final chiral (i.e., helical) complex produces two enantiomers and $\omega_{4,3}^{Eu,\mathbf{L4}}$ must be multiplied by two, thus the final statistical factor is $\omega_{4,3}^{chiral} \cdot \omega_{4,3}^{Eu,\mathbf{L4}} = 2 \cdot 1728 = 3456$. The same approach has been used for calculating the statistical factors of the complexes $[Eu_m(\mathbf{L4})_n]^{3m+}$ (Figure 4, entries 2–8), $[Eu_m(\mathbf{Lk})_n]^{3m+}$ ($k = 1$, 2, Figure S1, Supporting Information) and $[Eu_m(\mathbf{L3})_n]^{3m+}$ (Figure S2, Supporting Information). A simultaneous non-linear least-squares fit of Equation (S1–S13) (Supporting Information) modeling the experimental stability constants collected for the binuclear $[Eu_m(\mathbf{Lk})_n]^{3m+}$ ($k = 1$, 2),[8,9] and the trinuclear $[Eu_m(\mathbf{L3})_n]^{3m+}$ helicates,,[10,21] with now adequate statistical factors, provides a novel set of five microscopic parameters (Table 1, columns 3 and 4), for which the recalculated stability constants closely match the experimental data (Agreement Factor $AF = \sqrt{\sum_i (\log(\beta_{m,n,exp}^{Eu,\mathbf{Lk}}) - \log(\beta_{m,n,calcd}^{Eu,\mathbf{Lk}}))^2 / \sum_i (\log(\beta_{m,n,exp}^{Eu,\mathbf{Lk}}))^2} = 0.006$–$0.009$, Table 3, columns 4 and 5).

The choice of the dependence $c^{eff} \propto d^{-\alpha}$ ($\alpha = 1.5$ or 3) has only a marginal influence on the microscopic parameters (Table 1, columns 3 and 4) and their introduction into Equations (4), (6), (8), (10) yields predicted formation constants (Table 2, last line) characterizing the self-assembly of the tetranuclear helicate $[Eu_4(\mathbf{L4})_3]^{12+}$ [$\log(\beta_{4,3}^{Eu,\mathbf{L4}}) = 41.9$, Eq. (4)], and of its competitive complexes $[Eu_3(\mathbf{L4})_2]^{9+}$ [$\log(\beta_{3,2}^{Eu,\mathbf{L4}}) = 25.8$, Eq. (6)], $[Eu_3(\mathbf{L4})_3]^{9+}$ [$\log(\beta_{3,3}^{Eu,\mathbf{L4}}) = 36.2$, Eq. (8)] and $[Eu_4(\mathbf{L4})_2]^{12+}$ [$\log(\beta_{4,2}^{Eu,\mathbf{L4}}) = 31.3$, Eq. (4)]. The calculated predicted speciation at millimolar concentrations of ligand indicates that the target helicate $[Eu_4(\mathbf{L4})_3]^{12+}$ should correspond to more than 90% of the ligand speciation for a stoichiometric ratio Eu/**L4** 4:3 (Figure S3, Supporting Information); a strong point justifying the synthesis of the ligand **L4**.[15] We note that the apparent intermetallic repulsion $\Delta E_{1-2}^{EuEu} = 8$–$10\ kJ\,mol^{-1}$ (Table 1, columns 3 and 4) is much smaller than that calculated with the *Coulomb* interaction $\Delta E_{1-2,calcd}^{EuEu} = 9 \cdot N_{Av} \cdot e^2/4 \cdot \pi \cdot \varepsilon_0 \cdot \varepsilon_r \cdot d = 1388\ kJ \cdot mol^{-1}$ for two triply charged cations separated by $d = 9$ Å in a molecule ($N_{Av} = 6.02 \cdot 10^{23}\ mol^{-1}$, $e = 1.602 \cdot 10^{-19}$ C, $\varepsilon_0 = 8.859 \cdot 10^{-12}\ C\,N^{-1}\,m^{-2}$, $\varepsilon_r \approx 1.0$).[14] This deviation is mainly due to the contribution of solvation to the intermetallic interactions, which can be estimated with a Born–Haber cycle involving the solvation energies obtained with Born equation for the complexes $[Eu(\mathbf{L3})_3]^{3+}$ ($\Delta_{solv}G^0 = -607\ kJ\,mol^{-1}$), $[Eu_2(\mathbf{L3})_3]^{6+}$ ($\Delta_{solv}G^0 = -2208\ kJ\,mol^{-1}$) and $[Eu_3(\mathbf{L3})_3]^{9+}$ ($\Delta_{solv}G^0 = -4554\ kJ\,mol^{-1}$).[14] An exact fit to $\Delta E_{1-2}^{EuEu} = 9\ kJ\,mol^{-1}$ implies that the successive fixation of the metal ions in going from $[Eu(\mathbf{L3})_3]^{3+}$ to $[Eu_2(\mathbf{L3})_3]^{6+}$, and to $[Eu_3(\mathbf{L3})_3]^{9+}$, which is responsible for the increasing total charge of the complexes, is accompanied by a relative 13.8% stepwise increase of their pseudo-spherical sizes,[14] a value comparable to that previously reported for the successive fixation of three Cu^I cations in famous Lehn's double-stranded helicates (10%).[14]

Table 2. Experimental stability constants for $[Ln_m(\mathbf{L4})_n]^{3m+}$ (acetonitrile/dichloromethane 9:1, 298 K).

Ln^{III}	$\log(\beta_{3,3}^{Ln,\mathbf{L4}})$	$\log(\beta_{4,3}^{Ln,\mathbf{L4}})$	$\log(\beta_{3,2}^{Ln,\mathbf{L4}})$	$\log(\beta_{4,2}^{Ln,\mathbf{L4}})$
La	31.9(4)	39.1(1.5)	25.2(1.5)	30.4(1.5)
Nd	29.7(1.8)	38.4(1.9)	–	29.6(1.8)
Sm	29.7(1.5)	35.7(1.5)	–	–
Eu	36.8(1.5)	43.2(1.6)	28.9(1.4)	32.8(1.4)
Ho	34.5(1.5)	40.6(1.6)	26.3(1.4)	29.6(1.5)
Er	33.4(1.5)	38.1(1.5)	–	28.9(1.3)
Yb	32.5(1.5)	41.0(1.6)	26.5(1.3)	–
Lu	34.5(1.3)	40.8(1.3)	27.5(1.2)	31.1(1.2)
Eu[a]	36.2	41.9	25.8	31.3

[a] Predicted with Equations (4), (6), (8) and (10) and the microscopic parameters of Table 1 (columns 3 and 4).

Table 3. Experimental and fitted stability constants for $[Eu_m(\mathbf{Lk})_n]^{3m+}$ (simultaneous non-linear least-squares fits, acetonitrile, 298 K).

Species	$\log(\beta^{Eu,\mathbf{Lk}}_{m,n,exp})$[a]	$\log(\beta^{Eu,\mathbf{Lk}}_{m,n,calcd})$[b] $k=1$–3 Binomial statistics[c] $\alpha=3$[d]	$\log(\beta^{Eu,\mathbf{Lk}}_{m,n,calcd})$[b] $k=1$–3 Symmetry numbers $\alpha=3$[d]	$\log(\beta^{Eu,\mathbf{Lk}}_{m,n,calcd})$[b] $k=1$–3 Symmetry numbers $\alpha=1.5$[d]	$\log(\beta^{Eu,\mathbf{Lk}}_{m,n,calcd})$[b] $k=1$–4 Symmetry numbers $\alpha=3$[d]	$\log(\beta^{Eu,\mathbf{Lk}}_{m,n,calcd})$[b] $k=1$–4 Symmetry numbers $\alpha=1.5$[d]	$\log(\beta^{Eu,\mathbf{Lk}}_{m,n,calcd})$[b] $k=1$–4 Symmetry numbers[e]
$[Eu(\mathbf{L1})_2]^{3+}$	11.6(3)	11.4	11.4	11.3	11.4	11.2	12.2
$[Eu_2(\mathbf{L1})_2]^{3+}$	18.1(3)	18.3	18.3	18.3	18.6	18.6	18.3
$[Eu_2(\mathbf{L1})_3]^{6+}$	24.3(4)	24.2	24.2	24.3	24.1	24.3	25.0
$[Eu_2(\mathbf{L2})_2]^{6+}$	19.6(2)	19.5	19.5	19.4	19.8	19.8	18.3
$[Eu_2(\mathbf{L2})_3]^{6+}$	26.0(2)	26.1	26.1	26.0	25.8	26.0	25.0
$[Eu_2(\mathbf{L3})_3]^{6+}$	25.9(1.4)	26.1	26.1	26.3	25.9	26.3	26.8
$[Eu_3(\mathbf{L3})_2]^{9+}$	26.0(1.6)	26.1	26.0	26.1	26.6	26.9	26.0
$[Eu_3(\mathbf{L3})_3]^{9+}$	34.8(1.6)	34.7	34.7	34.6	34.7	35.1	34.0
$[Eu_3(\mathbf{L4})_2]^{9+}$	28.9(1.4)	–	–	–	28.2	27.7	29.8
$[Eu_4(\mathbf{L4})_2]^{12+}$	32.8(1.4)	–	–	–	32.6	32.8	33.0
$[Eu_3(\mathbf{L4})_3]^{9+}$	36.8(1.9)	–	–	–	37.2	35.8	37.2
$[Eu_4(\mathbf{L4})_3]^{12+}$	43.2(1.9)	–	–	–	43.2	43.5	43.0
AF[f]	–	0.006	0.006	0.009	0.012	0.02	0.03

[a] Experimental formation constants. [b] Computed using the fitted parameters in Table 1. [c] Taken from ref. [13b]. [d] Dependence of the effective concentration on the distance $c^{eff} \propto d^{-\alpha}$ ($\alpha=1.5$ or 3), see text. [e] Ercolani's model given in Equation (15). [f] Agreement factor, see text.

Experimental characterization of the self-assembly of the tetranuclear helicate $[Eu_4(\mathbf{L4})_3]^{12+}$ in solution: Electrospray-Ionization Mass Spectrometric (ESI-MS) titrations of **L4** (10^{-3} M) with $[Ln(CF_3SO_3)_3]\cdot xH_2O$ ($x=3$–5) in acetonitrile (Ln = La, Eu, Lu) are dominated by the signals of the saturated species $[Ln_4(\mathbf{L4})_3(CF_3SO_3)_n]^{(12-n)+}$ ($n=3$–9) together with signals arising from the unsaturated complexes $[Ln_3(\mathbf{L4})_3(CF_3SO_3)_n]^{(9-n)+}$ detected in excess of ligand (Ln/**L4** < 1.33), and $[Ln_3(\mathbf{L4})_2(CF_3SO_3)_n]^{(9-n)+}$ and $[Ln_4(\mathbf{L4})_2(CF_3SO_3)_n]^{(12-n)+}$ observed in excess of metal (Ln/**L4** > 1.33, Figure 6).

The parallel spectrophotometric batch titrations of **L4** ($2\cdot10^{-4}$ M) with $[Ln(CF_3SO_3)_3]\cdot xH_2O$ ($x=3$–5; Ln = La, Nd, Sm, Eu, Ho, Er, Yb, Lu) in acetonitrile/dichloromethane (9:1) show complicated variations of the absorption spectra (Ln/**L4** 0.1 to 4.0, Figure 7). Factor analysis[22] indicates the existence of at least five absorbing species corresponding to the free ligand **L4** and four complexes. Evolving factor analysis[23] suggests end points for Ln/**L4** 1.0, 1.3, 1.5 and 2.0, which match the stoichiometries of the various complexes detected in the gas phase during ESI-MS titrations. The spectrophotometric data can be satisfyingly fitted by using non-linear least-squares techniques[23] with the four absorbing complexes $[Ln_3(\mathbf{L4})_3]^{9+}$ [end point Ln/**L4** 1.0, Eq. (7)], $[Ln_4(\mathbf{L4})_3]^{12+}$ [end point Ln/**L4** 1.33, Eq. (2)], $[Ln_3(\mathbf{L4})_2]^{9+}$ (end point Ln/**L4** 1.5, Eq. (5)] and $[Ln_4(\mathbf{L4})_2]^{12+}$ [end point Ln/**L4** 2.0, Eq. (9)]. Because of the strong correlation between the calculated absorption spectra of these complexes, we were able to obtain a set of four independent macroscopic stability constants $\beta^{Eu,\mathbf{L4}}_{m,n}$ only for Ln = La, Eu, Ho and Lu, while partial data are available for the other lanthanides (Table 2).

Despite the uncertainties affecting the stability constants resulting from i) the use of a batch method required by the slow helicate formation (>24 h) and ii) the strong correlation between the absorption spectra of the four complexes, we can conclude that the experimental stability constants found for $[Eu_m(\mathbf{L4})_n]^{3m+}$ (Table 2, line 4) match fairly well those predicted from the microscopic parameters determined for the binuclear $[Eu_m(\mathbf{Lk})_n]^{3m+}$ ($k=1$, 2) and trinuclear $[Eu_m(\mathbf{L3})_n]^{3m+}$ complexes (Table 2, last line). The combination of these four experimental stability macroconstants ($\beta^{Eu,\mathbf{L4}}_{3,3}$,$\beta^{Eu,\mathbf{L4}}_{4,3}$,$\beta^{Eu,\mathbf{L4}}_{3,2}$ and $\beta^{Eu,\mathbf{L4}}_{4,2}$) reported here with the eight stability macroconstants previously collected for bi- and trinuclear complexes (Table 3)[13b] produces an extended set of twelve independent equations [constructed from Equations (S1–S13), Supporting Information together with Equations (4), (6), (8), (10)] for fitting five final microscopic parameters by non-linear least-squares (Table 1, columns 5 and 6). Again, we notice that the choice of the dependence $c^{eff} \propto d^{-\alpha}$ ($\alpha=1.5$ or 3) has only marginal effect on the microscopic parameters (Table 1, columns 5 and 6). The eventual repulsive character of the intermetallic $\Delta E^{EuEu}_{1-2} = 9$–10 kJ mol^{-1} and interligand $\Delta E^{LL}=6$–8 kJ mol^{-1} interactions confirm the occurrence of global anti-cooperative processes accompanying the formation of any complex in this family. Moreover, since i) the microscopic affinities are similar ($f^{Eu}_{N3} \approx f^{Eu}_{N2O}$) and ii) the intermetallic (ΔE^{EuEu}_{1-2}) and interligand (ΔE^{LL}) interactions are modest, the extended site-binding model [Eq. (1)] can be reduced to the original *Ercolani*'s model by setting $K_{inter}=f^{Eu}_{N3}=f^{Eu}_{N20}$, $K_{intra}=K_{inter}\cdot c^{eff}$ and $\Delta E^{EuEu}_{1-2}=\Delta E^{LL}=0$ [Eq. (15)].[12b]

$$\begin{aligned}\beta^{M,L}_{m,n} &= \omega^{chiral}_{m,n}\cdot\omega^{M,L}_{m,n}\cdot(K_{inter})^{m+n-1}\cdot(K_{inter}\cdot c^{eff}_i)^{mn-m-n+1}\\ &= \omega^{chiral}_{m,n}\cdot\omega^{M,L}_{m,n}\cdot(K_{inter})^{m+n-1}\cdot(K_{intra})^{mn-m-n+1}\end{aligned} \quad (15)$$

The simultaneous multi-linear least-squares fit of the twelve experimental formation constants collected for the helicates $[Eu_m(\mathbf{Lk})_n]^{3m+}$ ($k=1$–4, Table 1, column 2) with Equation (15) gives $\log(K_{inter})=4.93$ and $\log(K_{intra})=1.65$. The agreement between experimental and re-calculated con-

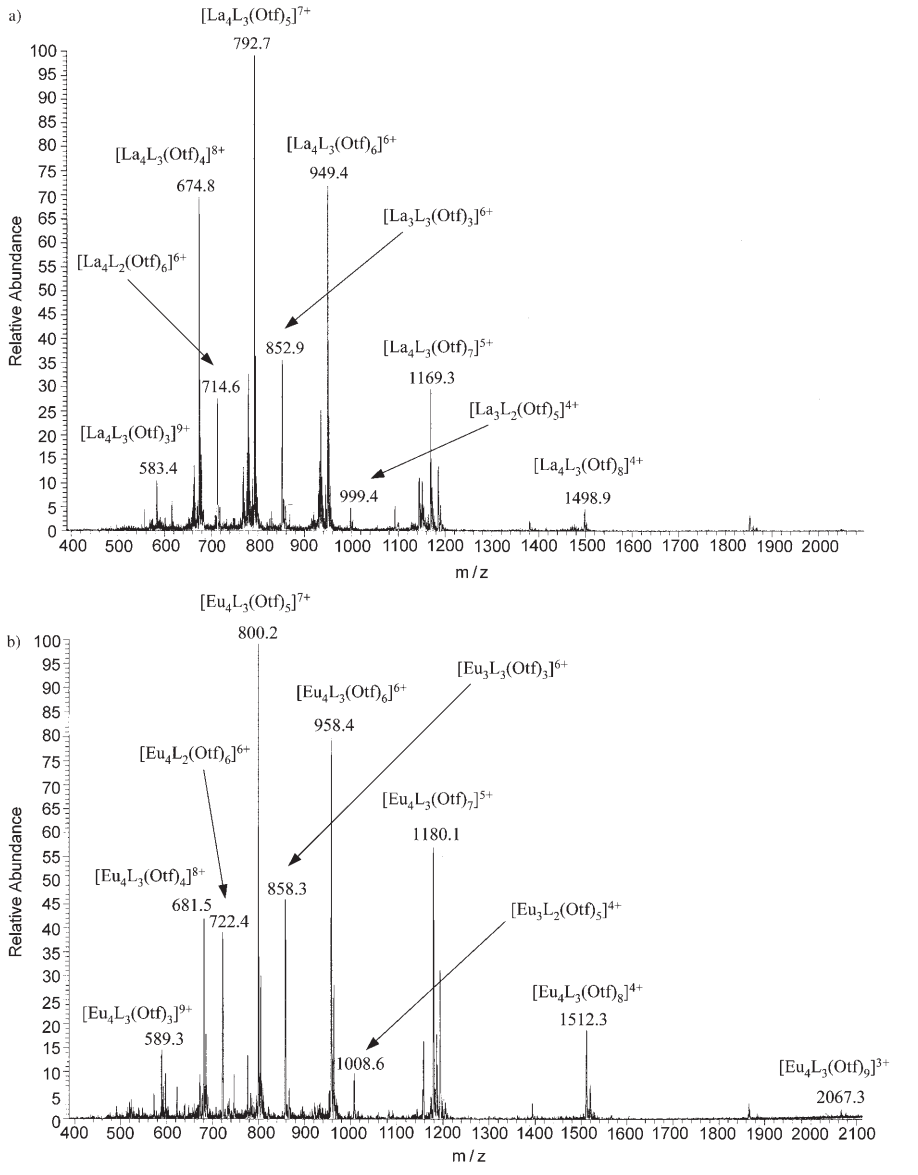

Figure 6. ESI-MS spectra recorded for Ln/**L4** = 1.33 (acetonitrile, Otf = $CF_3SO_3^-$, $|\mathbf{L4}|_{tot} = 10^{-3}$ M) with a) Ln = La, and b) Ln = Eu.

stants (Table 3, columns 1 and 8) are slightly less satisfying with this model (AF = 0.03), but its simplicity remains a very strong argument for its use as a first approximation of the energetics governing multi-component self-assembly processes.

The ^{1}H NMR spectra of the tetranuclear complexes $[Ln_4(\mathbf{L4})_3]^{12+}$ (Figure 8 and Figure S4, Supporting Information) systematically display 39 signals, which confirm the exclusive formation of the D_3-symmetrical triple-stranded helicates at millimolar concentrations.[15] The diagnostic downfield shifts of protons H3, H9 and H12 in the fast-relaxing paramagnetic $[Eu_4(\mathbf{L4})_3]^{12+}$ helicate points to the existence of a tight triple-stranded helix,[10] while the detailed analysis of two-dimensional COSY-, NOESY-, ROESY-NMR spectra allows the complete assignement of the 39 signals for the diamagnetic complexes $[La_4(\mathbf{L4})_3]^{12+}$ (Figure 8a) and $[Lu_4(\mathbf{L4})_3]^{12+}$ (Figure 8b).

Structural and photophysical properties of the self-assembled tetranuclear helicate $[Eu_4(\mathbf{L4})_3]^{12+}$ in the solid state: Isolation of the target tetranuclear helicate from concentrated methanol solutions with Ln/**L4** = 1.33 gives 70–85% yield of $[Ln_4(\mathbf{L4})_3](CF_3SO_3)_{12}\cdot x H_2O\cdot y CH_3OH$ (Ln = La: $x = 8.1$, $y = 1.6$; Ln = Eu: $x = 5.0$, $y = 2.3$; Ln = Gd: $x = 1.4$, $y = 0$; Ln = Tb: $x = 4.4$, $y = 5.2$; Ln = Lu: $x = 9.6$, $y = 4.7$, Table S1, Supporting Information).[15] The crystal structure of $[Eu_4(\mathbf{L4})_3]^{12+}$ unambiguously confirms the formation of the tetranuclear triple-stranded helicate (Figure 3), characterized by an almost linear arrangement of the metals (∢ Eu1···Eu2···Eu3 170.71(1)°, ∢ Eu2···Eu3···Eu4 172.03(1)°) combined with their regular spacing along the helical axis (Eu1···Eu2 9.312(1) Å, Eu2···Eu3 9.054(1) Å, Eu3···Eu4 9.405(1) Å, average Eu···Eu 9.26(18) Å).[15] The resulting palindromic helix is 31 Å long for 2.22 turns, which translates into an average 14.0 Å helical pitch, comparable with 13.6 Å previously reported for the trinuclear analogous complex $[Eu_3(\mathbf{L3})_3]^{9+}$.[10] The two terminal metals (Eu1 and Eu4) are nine-coordinated in pseudo-tricapped trigonal prismatic N_6O_3 sites, while the two central metals (Eu2 and Eu3) lie in pseudo-tricapped trigonal prismatic N_9 sites. Since we expect slightly different crystal-field parameters for these two environments,[10] a detailed photophysical analysis has been performed by using Eu^{III} as a structural and electronic probe in $[Eu_4(\mathbf{L4})_3]^{12+}$. The high-resolution excitation profile of the Eu($^5D_0 \leftarrow {}^7F_0$) transition in $[Eu_4(\mathbf{L4})_3]^{12+}$ at 10 K indeed confirms the existence of two main Eu^{III} sites, labeled I and II (Figure 9a). The most intense transition displays two main components, labeled Ia ($\bar{\nu} = 17221\ cm^{-1}$ at 10 K, $17225\ cm^{-1}$ at 295 K), and Ib (17215, $17227\ cm^{-1}$). Selectively excited emission spectra are, however, extremely similar, so that these two components are ascribed to a single metal ion environment I, the small differences evidenced probably arising from slight con-

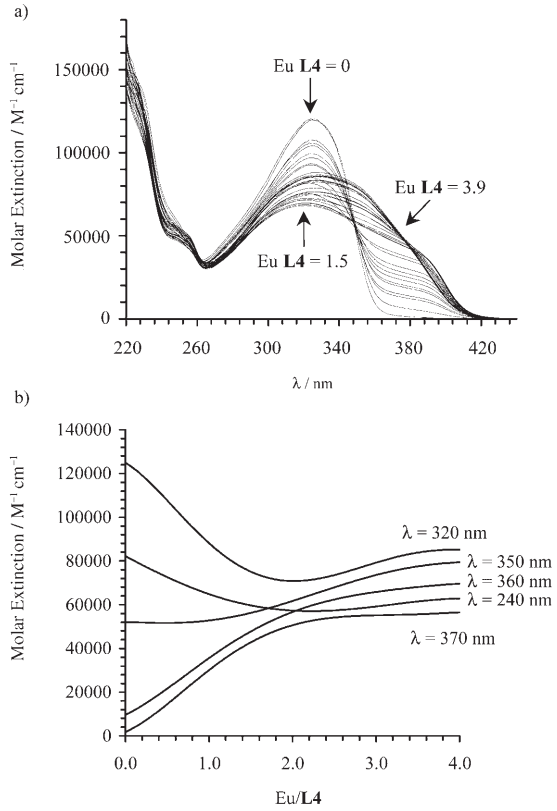

Figure 7. a) Variation of the absorption spectra observed during the spectrophotometric titration of **L4** with $Eu(CF_3SO_3)_3{\cdot}5H_2O$ ($|\mathbf{L4}|_{tot} = 2{\cdot}10^{-4}$ M, acetonitrile + 10% CH_2Cl_2, 298 K, Eu/**L4** 0.1–4.0). b) Corresponding variation of observed molar extinctions at five different wavelengths.

formational changes, a fact corroborated by the almost equal values of $\bar{\nu}$ for Ia and Ib at room temperature. In agreement with the detailed assignment previously established for the analogous complex $[Eu_3(\mathbf{L3})_3]^{9+}$ (site EuN_6O_3: 17219 cm^{-1} at 10 K),[10] this chemical environment is ascribed to the terminal N_6O_3 coordination sites. The associated emission spectrum recorded upon selective excitation of site I in $[Eu_4(\mathbf{L4})_3]^{12+}$ shows a crystal-field splitting compatible with a pseudo-D_3 symmetry around Eu^{III} (Figure 9b and Table S2, Supporting Information). The three observed transitions to the $^7F_1$ level can be labeled $A_1 \rightarrow A_2$ ($^7F_1(A_2)$ located at 312 cm^{-1} with respect to $^7F_0(A_1)$) and $A_1 \rightarrow$ split E (barycenter: 409 cm^{-1}, Figure S5, Supporting Information). The splitting of the E sublevel is related to the distortion from idealized D_3 symmetry and amounts to $\Delta E_{EE} =$ 38 cm^{-1}. These characteristics closely match those reported for the terminal EuN_6O_3 sites in $[Eu_3(\mathbf{L3})_3]^{9+}$ ($^7F_1(A_2) =$ 327 cm^{-1}, $^7F_1(E) = 402$ cm^{-1}, $\Delta E_{EE} = 42$ cm^{-1}), in agreement with very similar structural organizations of the EuN_6O_3 terminal sites in both triple-stranded helices.

The $Eu(^5D_0 \rightarrow {}^7F_2)$ transition in $[Eu_4(\mathbf{L4})_3]^{12+}$ shows roughly two groups of two emission bands assigned to the allowed electric dipole transitions $A_1 \rightarrow E$ in D_3 symmetry, the latter being further split into two components separated by ca. 20 cm^{-1} (Figure S6, Table S2, Supporting Information). Because of low-lying ligand-to-metal charge transfer (LMCT) states, which quench the $\mathbf{L4}(^3\pi\pi^*) \rightarrow Eu^{III}$ energy transfer responsible for metal-centred luminescence of EuN_9 sites,[10,25] the associated emission intensity of the central sites in $[Eu_4(\mathbf{L4})_3]^{12+}$ is very weak and cannot be observed upon broad band irradiation (Figure 9b). However, selective excitation of site II at 17235 cm^{-1} (10 K) produces a weak, but detectable emission spectrum reflecting trigonal symmetry, which is compatible with its attribution to EuN_9 (found at 17238 cm^{-1} in $[Eu_3(\mathbf{L3})_3]^{9+}$ under the same conditions).[10] Due to thermally-activated $EuN_9 \rightarrow EuN_6O_3$ energy migrations, the photophysical signature of site II disappears at 295 K, but we can estimate $\bar{\nu}(Eu(^5D_0 \leftarrow {}^7F_0)) = 17250$ cm^{-1} at 295 K by taking into account the 1 cm^{-1}/24 K dependence of this transition.[24] Application of eq 16, which empirically models the nephelauxetic effect produced by the donor atoms in the first coordination sphere,[26] predicts that $\bar{\nu}^{calcd}_{EuN6O3} = 17235$ cm^{-1} for a Eu^{III} atom coordinated by six heterocyclic nitrogen atoms ($\delta_{N\text{-heterocyclic}} = -15.3$ cm^{-1})[27] and three amide oxygen atoms ($\delta_{O\text{-amide}} = -15.7$ cm^{-1});[26] and $\bar{\nu}^{calcd}_{EuN9} = 17236$ cm^{-1} when Eu^{III} is coordinated by nine heterocyclic nitrogen atoms at 295 K ($\bar{\nu}_0 = 17374$ cm^{-1} is the energy of the $Eu(^5D_0 \leftarrow {}^7F_0)$ transition in the free ion, C_{CN} is an empirical coefficient depending on the coordination number of the metal, $C_{CN=8} = 1.06$, $C_{CN=9} = 1.0$, $C_{CN=10} = 0.95$ and δ_i represents the nephelauxetic effect produced by an atom i bound to Eu^{III}).[26]

$$\bar{\nu}^{calcd} = \bar{\nu}_0 + C_{CN} \cdot \sum_{i=1}^{CN} \nu_i \cdot \delta_i \qquad (16)$$

As previously noticed for $[Eu_3(\mathbf{L3})_3]^{9+}$,[10] predictions for both central and terminal Eu^{III} sites significantly deviate from the experimental values recorded for the $Eu(^5D_0 \leftarrow {}^7F_0)$ transitions at 295 K [Eqs. (17, 18)]. This observation suggests that pyridine and benzimidazole rings in ligand **L3** and **L4** possess different nephelauxetic parameters, in agreement with the substantial larger π-donating properties of benzimidazole rings, compared with pyridines.[28] The straightforward mathematical solution of Equations (17–18) gives $\delta_{N\text{-pyridine}} = -25.3$ cm^{-1} and $\delta_{N\text{-benzimidazole}} = -8.0$ cm^{-1}, a result in line with the expected larger capacity of pyridine rings to expand the metallic electronic cloud.[28]

$$\bar{\nu}^{exp}_{EuN6O3} = \bar{\nu}_0 + 3 \cdot \delta_{O\text{-carboxamide}} + 3 \cdot \delta_{N\text{-pyridine}} + 3 \cdot \delta_{N\text{-bzim}} = 17227 \text{ cm}^{-1} \qquad (17)$$

$$\bar{\nu}^{exp}_{EuN9} = \bar{\nu}_0 + 3 \cdot \delta_{N\text{-pyridine}} + 6 \cdot \delta_{N\text{-bzim}} = 17250 \text{ cm}^{-1} \qquad (18)$$

The $Eu(^5D_0)$ lifetimes in $[Eu_4(\mathbf{L4})_3]^{12+}$ at 10 K (2.00–2.24 ms, Table S3, Supporting Information) and at 295 K (1.63–1.74 ms, Table S3, Supporting Information) point to the absence of high-frequency oscillators (ν_{OH}, ν_{NH}) in direct contact with Eu^{III} in both types of coordination sites. Moreover, these spectroscopic and photophysical characteristics still hold for millimolar acetonitrile solutions of $[Eu_4(\mathbf{L4})_3]^{12+}$,

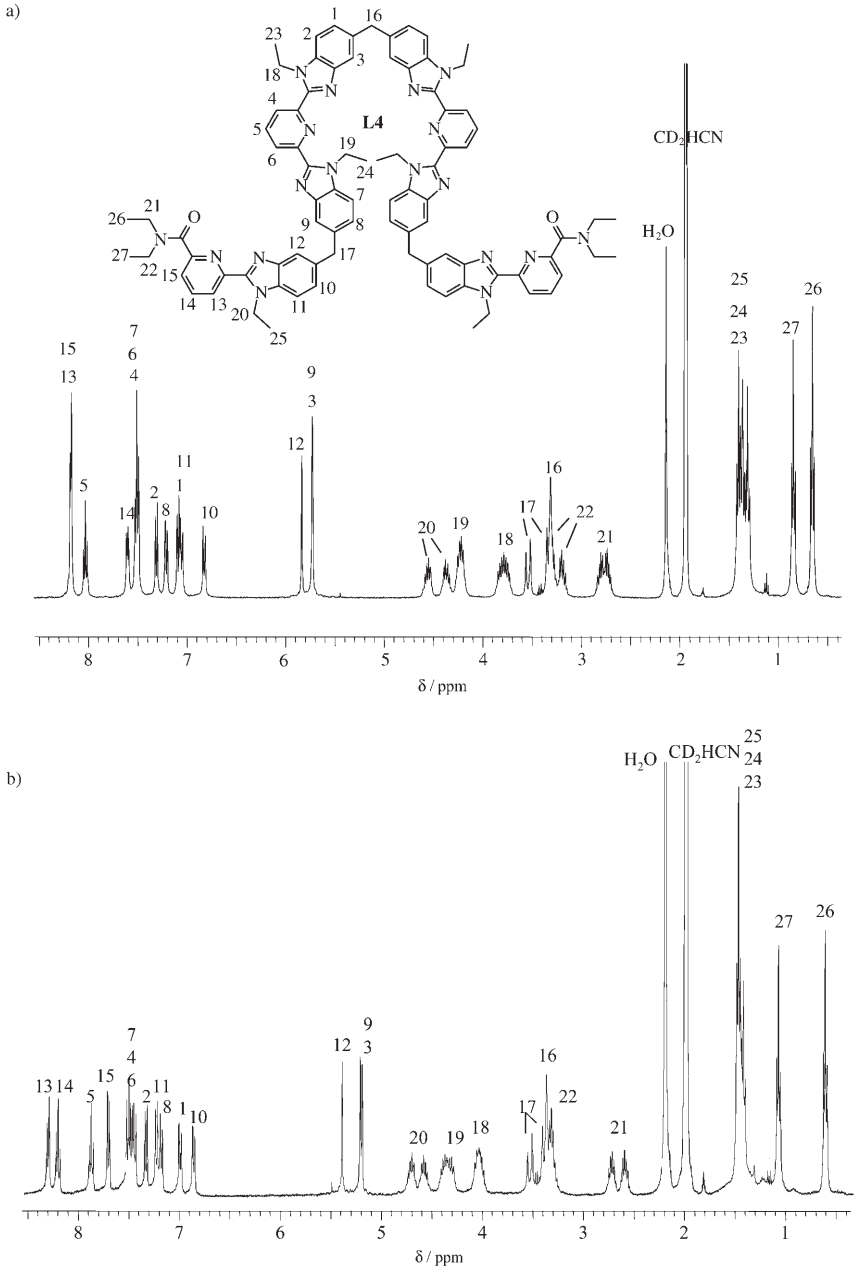

Figure 8. a) ^{1}H NMR spectra with complete assignment for a) $[La_4(\mathbf{L4})_3]^{12+}$ and b) $[Lu_4(\mathbf{L4})_3]^{12+}$ (CD_3CN/CD_2Cl_2 95:5, 298 K).

which demonstrates that the tetranuclear triple-stranded helical structure is maintained in solution. Finally, Table 4 summarizes the main photophysical characteristics of the ligand-centred $^1\pi\pi^*$ and $^3\pi\pi^*$ excited states in **L4**, which closely resemble those reported previously for **L3** ($E(^1\pi\pi^*) = 23\,000$ cm^{-1}, $E(^3\pi\pi^*) = 19\,800$–$20\,000$ cm^{-1}).[10]

Conclusion

The formation of stable tetranuclear helicates $[Ln_4(\mathbf{L4})_3]^{12+}$ in condensed phase demonstrates that highly charged molecular systems ($Q = \Sigma q$, q is the charge borne per metal) do not drastically suffer from the large internal electrostatic repulsion $\Delta_{elec}G^{MM} \propto \Sigma(q^2/r)$, as long as the total size of the microscopic objects (approximate spherical radius R) is adapted for providing solvation energies $\Delta_{solv}G\alpha Q^2/R$, which are able to balance the latter repulsion in polar solvents.[14] This phenomenon may explain the self-assembly of linear helicates based on Cu^I,[29] or of trivalent lanthanides ($[Ln_2(\mathbf{Lk})_3]^{6+}$ ($k = 1$, 2), $[Ln_3(\mathbf{L3})_3]^{9+}$, and $[Ln_4(\mathbf{L4})_3]^{12+}$ in this contribution). The alternative recurrent argument invoking strong ion-pairing for stabilizing highly charged objects in solution does not agree with a simple calculation of the charge density on the Connolly surface around the cation,[30] which amounts to 9/1682.6 = $5.35\cdot10^{-3}$ eu Å^{-2} for $[Eu_3(\mathbf{L3})_3]^{9+}$ and 12/2044 = $5.83\cdot10^{-3}$ eu Å^{-2} for $[Eu_4(\mathbf{L4})_3]^{12+}$, while that obtained for Na^+ ($4.35\cdot10^{-2}$ eu Å^{-2}), Ca^{2+} ($7.22\cdot10^{-2}$ eu Å^{-2}) and La^{3+} ($8.85\cdot10^{-3}$ eu Å^{-2}) are one order of magnitude larger.[31] With this observation in mind, the use of statistical factors adapted to self-assembly processes mixing intra- and intermolecular connections combined with simple additive thermodynamic site-binding models,[11,13] provides an efficient tool for predicting stabilities of target supramolecular complexes within a family, for which basic microscopic parameters can be estimated. In this context, the a priori prediction (and experimental confirmation) of the quantitative formation of $[Eu_4(\mathbf{L4})_3]^{12+}$ at millimolar concentration is unprecedented in coordination and metallosupramolecular chemistry. Moreover, the deeper understanding of the thermodynamic driving forces controlling multi-component self-assembly processes, among which tuneable intermetallic interactions play a crucial role, opens

Table 4. Ligand-centred absorption and emission properties of **L4** and of its complexes $[Ln_4(\mathbf{L4})_3](CF_3SO_3)_{12}$ (Ln = Eu, Gd, Tb) in the solid state.[a]

Compound	T [K]	Absorption [cm^{-1}] $\pi\rightarrow\pi^*$	Emission [cm^{-1}] $^1\pi\pi^*$	Emission [cm^{-1}] $^3\pi\pi^*$	Lifetime [ms] $\tau(^3\pi\pi^*)$
L4	295	30660	23980 sh 20880	–	–
	77		23260 sh 21010	19840 sh 18350	[b]
$[Gd_4(\mathbf{L4})_3](CF_3SO_3)_{12}$	295	31150 25640 sh	22270	19000br	[b]
	77		22730	20040 sh 18690 17421 sh	1.11(1)
$[Eu_4(\mathbf{L4})_3](CF_3SO_3)_{12}$	295	30580 25640 sh	[c]	[c]	
	77		[c]	[c]	
$[Tb_4(\mathbf{L4})_3](CF_3SO_3)_{12}$	295	31150 25640 sh	[c]	19000br	[b]
	77		[c]	[c]	

[a] sh = shoulder, br = broad. [b] The intensity is too weak to obtain reliable lifetime measurements. [c] Ligand-centred luminescence quenched by transfer to Ln ion.

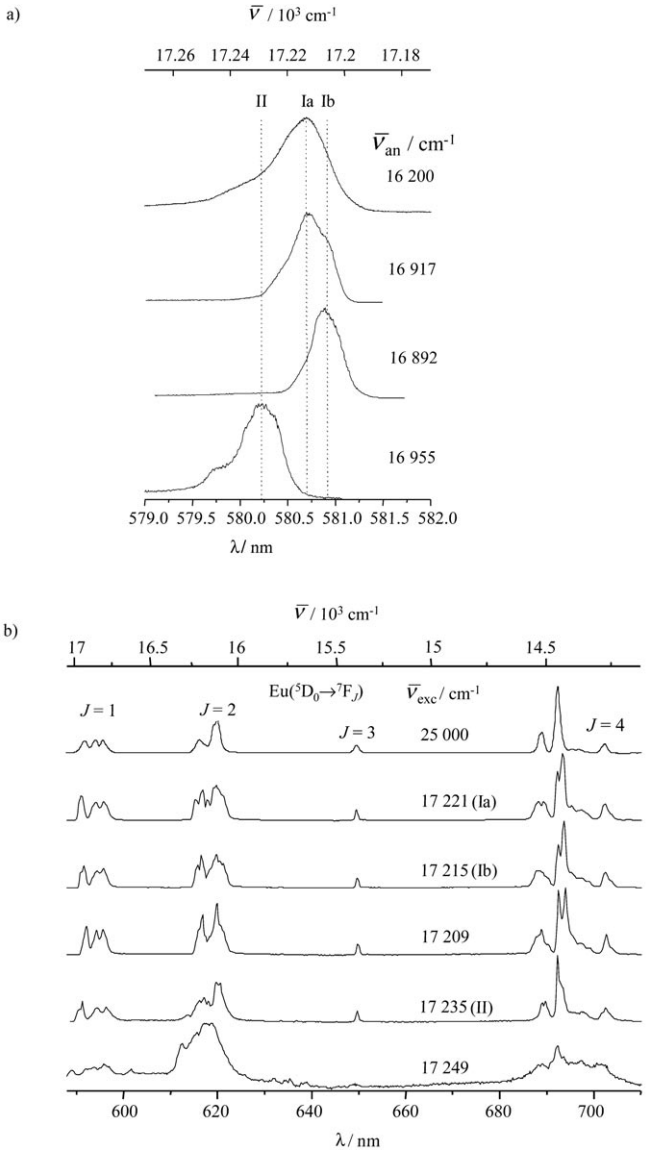

Figure 9. a) High-resolution excitation profiles of the $Eu(^5D_0\leftarrow{}^7F_0)$ transitions in $[Eu_4(\mathbf{L4})_3](CF_3SO_3)_{12}$ recorded at different analysing wavelengths (solid-state, 10 K). b) Emission spectra obtained upon broad band and selective excitations in $[Eu_4(\mathbf{L4})_3](CF_3SO_3)_{12}$ (solid state, 10 K).

novel perspectives for addressing the unsolved chemical challenge of selectively introducing different lanthanides possessing very similar coordination properties, but slightly different sizes, into an organized linear polymetallic chain.

Experimental Section

Chemicals were purchased from Fluka AG and Aldrich, and used without further purification unless otherwise stated. The ligand **L4** and its complexes $[Ln_4(\mathbf{L4})_3](CF_3SO_3)_{12}\cdot x H_2O\cdot y CH_3OH$ (Ln = La: $x = 8.1$, $y = 1.6$; Ln = Eu: $x = 5.0$, $y = 2.3$; Ln = Gd: $x = 1.4$, $y = 0$; Ln = Tb: $x = 4.4$, $y = 5.2$; Ln = Lu: $x = 9.6$, $y = 4.7$) were prepared according to literature procedures.[15] $Ln(CF_3SO_3)_3\times x H_2O$ (Ln = La–Lu)[32] were prepared from the corresponding oxides (Aldrich, 99.99%). The Ln content of solid salts was determined by complexometric titrations with Titriplex III (Merck) in the presence of urotropine and xylene orange.[33] Acetonitrile and dichloromethane were distilled over calcium hydride.

Spectroscopic and analytical measurements: Electronic spectra in the UV/Vis were recorded at 20°C from batch solutions in CH_3CN/CH_2Cl_2 9:1 with a Perkin–Elmer Lambda 900 spectrometer using quartz cells of 1 mm path length. Mathematical treatment of the spectrophotometric data was performed with factor analysis[22] and with the SPECFIT program.[23] IR spectra were obtained from KBr pellets with a FT-IR Perkin-Elmer Spectrum One. ^1H and ^{13}C NMR spectra were recorded at 25°C on a Bruker Avance 400 MHz and Bruker DRX-500 MHz spectrometers. Chemical shifts are given in ppm with respect to TMS. Pneumatically-assisted electrospray (ESI-MS) mass spectra were recorded from 10^{-4} mol dm^{-3} solutions on a Finnigan SSQ7000 instrument. The equipment and experimental procedures for luminescence measurements in the visible range were published previously.[34] Excitation of the finely powdered samples was achieved by a 300 W xenon high-pressure lamp coupled with a monochromator or a Coherent Innova Argon laser. The emitted light was analyzed at 90° with a Spex 1404 double monochromator with holographic gratings (band-pass used 0.01–0.2 nm). Emitted photon flux was measured with a Hamatsu R-943-02 photomultiplier with a cooled CaAs(Cs) photocathode (−20°C), coupled to a home-built linear amplifier (440 MHz) and a Stanford Research SR-400 double photon counter. The emission spectra were corrected for the instrumental response. Luminescent lifetimes were measured using excitation provided by a Quantum Brillant Nd/YAG laser equipped with frequency doubler, tripler and quadrupler as well as with an OPOTEK MagicPrism OPO crystal. Selective excitations of the 0–0 profiles were performed by means of a Continuum MD 6000 dye laser pumped at 532 nm. The output signal of the photomultiplier was fed into a Stanford Research SR-430 multichannel scaler and transferred to a PC. Lifetimes are averages of three independent determinations. Computations of the concentrations were performed with the HySS2 program (Protonic software). Least-squares fitting methods were implemented in Excel and Mathematica. Elemental analyses were performed by Dr. H. Eder from the Microchemical Laboratory of the University of Geneva.

Acknowledgement

Financial support from the COST D31 action and from the Swiss National Science Foundation is gratefully acknowledged.

[1] a) J.-M. Lehn, in *Supramolecular Chemistry/Science. Some Conjectures and Perspectives* (Eds.: R. Ungaro, E. Dalcanale), Kluwer Academic Publishers, **1999**, p. 287–304; b) G. M. Whitesides, *Chem. Rev.* **2005**, *105*, 1171–1196; c) V. Balzani, A. Credi, M. Venturi, *Chem. Eur. J.* **2002**, *8*, 5525–5532.

[2] V. Balzani, G. Bergamini, F. Marchioni, P. Ceroni, *Coord. Chem. Rev.* **2006**, *250*, 1254–1266.

[3] a) S. J. Cantrill, A. R. Pease, J. F. Stoddart, *J. Chem. Soc. Dalton Trans.* **2000**, 3715–3734; b) E. R. Kay, D. A. Leigh, F. Zerbetto, *Angew. Chem.* **2007**, *119*, 72–196; *Angew. Chem. Int. Ed.* **2007**, *46*, 72–191.

[4] A. Mulder, J. Huskens, D. N. Reinhoudt, *Org. Biomol. Chem.* **2004**, *2*, 3409–3424.

[5] C. Piguet, J.-C. G. Bünzli, B. Donnio, D. Guillon, *Chem. Commun.* **2006**, 3755–3768.

[6] a) J. D. Badjic, A. Nelson, S. J. Cantrill, W. B. Turnbull, J. F. Stoddart, *Acc. Chem. Res.* **2005**, *38*, 723–732; b) G. Ercolani, *Struct. Bonding (Berlin)* **2006**, *121*, 167–215.

[7] a) G. Koper, M. Borkovec, *J. Phys. Chem. B* **2001**, *105*, 6666–6674; b) M. Borkovec, J. Hamacek, C. Piguet, *Dalton Trans.* **2004**, 4096–4105; c) M. Borkovec, G. J. M. Koper, C. Piguet, *Curr. Opin. Colloid Interface Sci.* **2006**, *11*, 280–289.

[8] C. Piguet, J.-C. G. Bünzli, G. Bernardinelli, G. Hopfgartner, A. F. Williams, *J. Am. Chem. Soc.* **1993**, *115*, 8197–8206.

[9] K. Zeckert, J. Hamacek, J.-P. Rivera, S. Floquet, A. Pinto, M. Borkovec, C. Piguet, *J. Am. Chem. Soc.* **2004**, *126*, 11589–11601.

[10] S. Floquet, N. Ouali, B. Bocquet, G. Bernardinelli, D. Imbert, J.-C. G. Bünzli, G. Hopfgartner, C. Piguet, *Chem. Eur. J.* **2003**, *9*, 1860–1875.

[11] a) C. Piguet, M. Borkovec, J. Hamacek, K. Zeckert, *Coord. Chem. Rev.* **2005**, *249*, 705–726; b) J. Hamacek, M. Borkovec, C. Piguet, *Dalton Trans.* **2006**, 1473–1490.

[12] a) G. Ercolani, *J. Phys. Chem. B* **2003**, *107*, 5052–5057; b) G. Ercolani, *J. Am. Chem. Soc.* **2003**, *125*, 16097–16103.

[13] a) J. Hamacek, M. Borkovec, C. Piguet, *Chem. Eur. J.* **2005**, *11*, 5217–5226; b) J. Hamacek, M. Borkovec, C. Piguet, *Chem. Eur. J.* **2005**, *11*, 5227–5237.

[14] G. Canard, C. Piguet, *Inorg. Chem.* **2007**, *46*, 3511–3522.

[15] K. Zeckert, J. Hamacek, J.-M. Senegas, N. Dalla-Favera, S. Floquet, G. Bernardinelli, C. Piguet, *Angew. Chem.* **2005**, *117*, 8168–8172; *Angew. Chem. Int. Ed.* **2005**, *44*, 7954–7958.

[16] a) W. Kuhn, *Kolloid Z.* **1934**, *68*, 2–15; b) H. Jacobson, W. H. Stockmayer, *J. Chem. Phys.* **1950**, *18*, 1600–1606; c) P. J. Flory, U. W. Suter, M. Mutter, *J. Am. Chem. Soc.* **1976**, *98*, 5733–5739; d) W. P. Jencks, *Proc. Natl. Acad. Sci. USA* **1981**, *78*, 4046–4050; e) M. A. Winnik, *Chem. Rev.* **1981**, *81*, 491–524; f) J. M. Gargano, T. Ngo, J. Y. Kim, D. W. K. Acheson, W. J. Lees, *J. Am. Chem. Soc.* **2001**, *123*, 12909–12910; g) R. H. Kramer, J. W. Karpen, *Nature* **1998**, *395*, 710–713; h) P. I. Kitov, D. R. Bundle, *J. Am. Chem. Soc.* **2003**, *125*, 16271–16284.

[17] G. Ercolani, M. Borkovec, J. Hamacek, C. Piguet, *J. Phys. Chem. B* **2007**, *111*, 12195–12203.

[18] a) S. W. Benson, *J. Am. Chem. Soc.* **1958**, *80*, 5151–5154; b) S. W. Benson, *Thermochemical Kinetics*, 2nd ed., Wiley-Interscience, New York, **1976**, pp. 37–39; c) W. f. Bailey, A. S. Monahan, *J. Chem. Educ.* **1978**, *55*, 489–493.

[19] D. M. Bishop, K. Laidler, *J. Chem. Phys.* **1965**, *42*, 1688–1691.

[20] For the sake of simplicity in calculating symmetry numbers, we consider that Eu^{III} exists in acetonitrile strictly as the tricapped trigonal prismatic complex $[Eu(CH_3CN)_9]^{3+}$, although it has been experimentally demonstrated that the main species in equilibrium in lanthanide triflate solutions in acetonitrile are $[Ln(Otf)_2(CH_3CN)_x]^+$ and $[Ln(OTf)_3(CH_3CN)_y]$, see P. Di Bernardo, G. R. Choppin, R. Portanova, P. L. Zanonato, *Inorg. Chim. Acta* **1993**, *207*, 85.

[21] S. Floquet, M. Borkovec, G. Bernardinelli, A. Pinto, L.-A. Leuthold, G. Hopfgartner, D. Imbert, J.-C. G. Bünzli, C. Piguet, *Chem. Eur. J.* **2004**, *10*, 1091–1105.

[22] E. R. Malinowski, D. G. Howery, *Factor Analysis in Chemistry*, Wiley, New York, Chichester, **1980**.

[23] a) H. Gampp, M. Maeder, C. J. Meyer, A. Zuberbühler, *Talanta* **1985**, *32*, 1133–1139; b) H. Gampp, M. Maeder, C. J. Meyer, A. Zuberbühler, *Talanta* **1986**, *33*, 943–951.

[24] J.-C. G. Bünzli, in *Lanthanide Probes in Life, Chemical and Earth Sciences* (Eds.: J.-C. G. Bünzli, G. R. Choppin), Elsevier, Amsterdam, **1989**, Chapter 7.

[25] S. Petoud, J.-C. G. Bünzli, C. Piguet, Q. Xiang, R. Thummel, *J. Lumin.* **1999**, *82*, 69–79.

[26] S. T. Frey, W.deW. Horrocks, *Inorg. Chim. Acta* **1995**, *228*, 383–390.

[27] a) C. Piguet, E. Rivara-Minten, G. Hopfgartner, J.-C. G. Bünzli, *Helv. Chim. Acta* **1995**, *78*, 1541–1566; b) C. Piguet, J.-C. G. Bünzli, G. Bernardinelli, G. Hopfgartner, S. Petoud, O. Schaad, *J. Am. Chem. Soc.* **1996**, *118*, 6681–6697.

[28] a) M.-A. Haga, T. Takasugi, A. Tomie, M. Ishizuya, T. Yamada, M. D. Hossain, M. Inoue, *Dalton Trans.* **2003**, 2069–2079; b) S. Torelli, S. Delahaye, A. Hauser, G. Bernardinelli, C. Piguet, *Chem. Eur. J.* **2004**, *10*, 3503–3516.

[29] a) J.-M. Lehn, A. Rigault, *Angew. Chem.* **1988**, *100*, 1121–1122; *Angew. Chem. Int. Ed. Engl.* **1988**, *27*, 1095–1096; b) K. T. Potts, M. Keshavarz-K. , F. S. Tham, H. D. Abruña, C. Arana, *Inorg. Chem.* **1993**, *32*, 4422–4435; c) K. T. Potts, M. Keshavarz-K. , F. S. Tham, H. D. Abruña, C. Arana, *Inorg. Chem.* **1993**, *32*, 4436–4449; d) K. T. Potts, M. Keshavarz-K. , F. S. Tham, H. D. Abruña, C. Arana, *Inorg. Chem.* **1993**, *32*, 4450–4456; e) K. T. Potts, M. Keshavarz-K, F. S. Tham, K. A. Gheysen Raiford, C. Arana, H. D. Abruña, *Inorg. Chem.* **1993**, *32*, 5477–5484; f) A. Marquis-Rigault, A. Dupont-Gervais, A. Van Dorsselaer, J.-M. Lehn, *Chem. Eur. J.* **1996**, *2*, 1395–1398.

[30] a) M. L. Connolly, *Science* **1983**, *221*, 709–713; b) M. L. Connolly, *J. Appl. Crystallogr.* **1983**, *16*, 548–553.

[31] The ionic radii of the cations in the gas phase have been used for estimating their Connolly surfaces ($R_{Na^+}=1.352$ Å, $R_{Ca^{2+}}=1.48$ Å and $R_{La^{3+}}=1.642$ Å, R. H. Stokes, *J. Am. Chem. Soc.* **1964**, *86*, 979–982).

[32] J. F. Desreux, in *Lanthanide Probes in Life, Chemical and Earth Sciences* (Eds.: J.-C. G. Bünzli, G. R. Choppin), Elsevier, Amsterdam, **1989**, Chapter 2.

[33] G. Schwarzenbach, *Complexometric Titrations*, Chapman & Hall, London, **1957**, p. 8.

[34] R. Rodriguez-Cortinas, F. Avecilla, C. Platas-Iglesias, D. Imbert, J.-C. G. Bünzli, A. de Blas, T. Rodriguez-Blas, *Inorg. Chem.* **2002**, *41*, 5336–5349.

Received: September 14, 2007
Published online: February 21, 2008

